J. Electrochem. Sci. Eng. **15(1)** (2025) 2522; http://dx.doi.org/10.5599/jese.2522

Open Access : : ISSN 1847-9286
https://pub.iapchem.org/ojs/index.php/JESE

Original scientific paper

Self-healing efficiency of ceria-doped Zn-Co coatings: Insights into particle-free *versus* biphasic plating baths

Marija Mitrović[1,✉], Anđela Simović[2], Regina Fuchs-Godec[3], Milorad Tomić[1,4] and Jelena Bajat[5]

[1]*University of East Sarajevo, Faculty of Technology Zvornik, Karakaj 34A 75400 Zvornik, Republic of Srpska, Bosnia and Herzegovina*
[2]*University of Belgrade, Institute of Chemistry, Technology and Metallurgy, National Institute of the Republic of Serbia, Njegoševa 12, 11000 Belgrade, Serbia*
[3]*University of Maribor, Faculty of Chemistry and Chemical Engineering, Smetanova ulica 17, 2000 Maribor, Slovenia*
[4]*Engineering Academy of Serbia, Kneza Miloša 9/I, 11000 Belgrade, Serbia*
[5]*University of Belgrade, Faculty of Technology and Metallurgy, Karnegijeva 4, 11000 Belgrade, Serbia*

Corresponding authors: ✉*marija.ridjosic@tfzv.ues.rs.ba; Tel.: 0038756260190; Fax: 0038756260190*

Received: October 8, 2024; Accepted: October 23, 2024; Published: October 26, 2024

Abstract

Achieving the superior properties of nanocomposite materials involves addressing several challenges, particularly the agglomeration of nanoparticles in the plating bath. This study focuses on the electrodeposition and characterization of Zn-Co-CeO_2 composite coatings using a particle-free plating bath, an effective strategy for mitigating agglomeration. For comparison, the composite coatings were also deposited from a traditional biphasic plating solution. The coatings were deposited galvanostatically at various current densities. Scanning electron microscopy revealed that using a particle-free plating solution in conjunction with lower current densities enhanced the compactness and the overall quality of the coatings. Lower current densities favoured the codeposition of particles, as indicated by energy-dispersive X-ray spectroscopy results. Notably, the coatings produced from the particle-free bath exhibited significantly improved corrosion resistance and durability in chloride-rich environments, attributed to their self-healing properties, as shown by electrochemical impedance spectroscopy.

Keywords

Zn-Co-CeO_2; smart nanomaterials; self-repair; ceria-doping; nanocomposite

Introduction

The electrodeposition of nanocomposite coatings has emerged as a significant area of research within materials engineering, owing to their versatile applications and the ability to tailor properties for specific uses. While various methods exist for producing nanocomposite coatings, electrodeposition offers distinct advantages, including operation at room temperature, precise control over coating thickness, applicability to complex geometries, and reduced equipment costs.

However, the electrochemical deposition of composite coatings is influenced by numerous parameters. These include the composition of the deposition solution (specifically the concentration of metal ions and particles), characteristics of the particles (such as size, shape, and surface charge), the presence of additives, pH levels, and deposition parameters (including deposition mode, potential, current density, temperature, and agitation) [1-10]. Additionally, the geometry of the electrodes and the deposition solution plays a critical role in the process. A significant challenge in electrochemical deposition is the low dispersion stability of particles in high ionic strength solutions, which can lead to particle agglomeration in biphasic media [11-14]. To mitigate this issue, several techniques have been employed, including mechanical mixing and wet ball milling prior to or during deposition. Ultrasonic mixing has also proven effective in preventing agglomeration and enhancing the properties of nanocomposite coatings [15-22]. Nonetheless, despite these methods, the inherent tendency of nanoparticles to agglomerate poses ongoing challenges, often resulting in rough, porous, and poorly distributed coatings. This non-uniformity can induce microstress in the coating and reduce key properties such as hardness, wear and corrosion resistance.

In terms of corrosion protection, ceria particles have demonstrated efficacy as corrosion inhibitors and are frequently integral to self-healing materials [23-29]. Self-healing materials are categorized as smart materials capable of autonomously repairing microscopic damage without external intervention. This inherent ability to self-repair enhances the longevity and durability of materials, making ceria-based composites particularly valuable in applications requiring sustained performance under harsh conditions. Ceria conversion films deposited via cathodic electrodeposition on steel, aluminium, pure zinc and zinc alloys exhibit high corrosion resistance [30,31]. Moreover, Zn-CeO_2 composite coatings demonstrate enhanced corrosion protection compared to pure zinc coatings [32-34]. The incorporation of ceria into the zinc and zinc alloy matrix imparts self-healing properties, which are critical for addressing the primary limitation of zinc coatings: their durability in corrosive environments.

Thus, the goal of this study is to produce Zn-Co-CeO_2 composite coatings from a particle-free deposition solution and to compare their morphology, composition, and corrosion resistance with those of coatings produced from biphasic solutions. This approach may address the main challenge in the composite production field, particle agglomeration and enhance the overall performance of composite coatings. Also, the aim of this study is the optimization of the deposition current density, which is a critical parameter influencing the amount of particles incorporated into the metal matrix [35-37]. While it is generally observed that particle content tends to increase with increasing current density and particle loading in the bath until a saturation point is reached, establishing a direct correlation between current density and particle content can be complex and may vary significantly based on the specific particles used. In some cases, the incorporation rate of particles may continuously decrease or display a peak as current density increases [12,38,39]. This behaviour is closely related to the dynamics of metal deposition and highlights the need for careful optimization to achieve the desired particle distribution within the coating and final properties of the coating.

Experimental

The preparation of AISI-1010 steel plates for the coating deposition process involves several steps. Initially, the steel is ground using silicon carbide abrasive paper of varying grits (No. 600, 800, 1000). This is followed by rinsing with distilled water, degreasing in a saturated NaOH solution in ethanol for 30 seconds, and then rinsing again with distilled water. The substrates are then etched in a HCl:H_2O (1:1 v/v) solution for 30 seconds and subsequently rinsed with distilled water. Composite coatings are deposited at various current densities: j = 1, 2, 3, 5, and 8 A dm^{-2}. A zinc anode with a purity of 99.99% is employed during the deposition. Two distinct solutions containing different sources of cerium ions (pH 5.5) are used. All used chemicals were analytical grade and produced by Sigma Aldrich. Both deposition solutions contain the following components: 0.1 M $ZnCl_2$; 0.8 M H_3BO_3; 3 M KCl; 0.03 M $CoCl_2$. In particle-free solution, 2 g/L of $CeCl_3$ is added, while the biphase solution contains 2 g/L of solid CeO_2 particles (particles size <50nm, according to producer). The plating solutions were stirred during the deposition by a magnetic stirrer at 300 rpm in order to minimize particle agglomeration. Also, the solutions were stirred for 10 minutes before electrodeposition to ensure the homogeneous distribution of particles in the plating solution throughout the deposition process. The deposition time for the composite coatings was calculated based on Faraday's law to achieve a target thickness of 10 µm. The morphology of the composite coatings was examined by scanning electron microscopy (SEM) (Tescan Mira) and composition was determined by energy dispersive X-ray spectroscopy (EDAX). Corrosion testing of the composite coatings is performed using a ZRA Reference 600 potentiostat from Gamry Instruments, utilizing electrochemical impedance spectroscopy (EIS) for analysis. The impedance spectra are recorded within a Faraday cage at the open circuit potential, spanning a frequency range of 100 kHz to 10 mHz, with an alternating voltage amplitude of 10 mV. A platinum mesh is employed as the counter electrode, while a saturated calomel electrode serves as the reference electrode, positioned in a Luggin capillary opposite the sample. The experimental data are subsequently analysed and fitted using the Gamry Echem Analyst software.

Results and discussion

Morphology of composite coatings

The morphology of electrodeposited composite coatings as a function of the deposition current density, as well as a function of the type of the Ce source, is shown in Figures 1 and 2. The morphology of the composite coatings produced at the lowest tested current density (1 A dm^{-2}) exhibited significant heterogeneity. The coating surface displayed irregularly distributed agglomerates interspersed with smaller structures. An increase in the deposition current density to 2 and 3 A dm^{-2} resulted in a more uniform and globular surface morphology characterized by grains of consistent size, albeit with pronounced porosity. At a further increase to 5 A dm^{-2}, the coatings developed smaller agglomerates. The furrows and cavities on the surface are likely attributed to the intense hydrogen evolution during the deposition process. In coatings utilizing CeO_2 solid participles as a source of Ce, higher current densities lead to the formation of increasingly inhomogeneous structures. Notably, the initially smooth and compact morphology observed at lower current densities transitions to a rougher and more irregular surface as deposition current density rises. At a current density of 5 A dm^{-2}, the emergence of cauliflower-like structures is evident, with these agglomerates exhibiting larger sizes that progressively coalesce into larger formations over time. This phenomenon is likely attributable to the uneven distribution of current density across the coating surface. As protrusions develop, ions preferentially undergo reduction at these elevated points, which consequently results in a greater

variety of irregular morphologies during the deposition process. The increase in deposition current density to 8 A dm^{-2} leads to heterogeneous morphology with visible CeO_2 agglomerates on the coating surface. The EDAX spot analyses of the white agglomerates on the surface (Figure 2 (e)) verify the presence of cerium, confirming the considerable agglomeration phenomenon present in the biphasic plating solution.

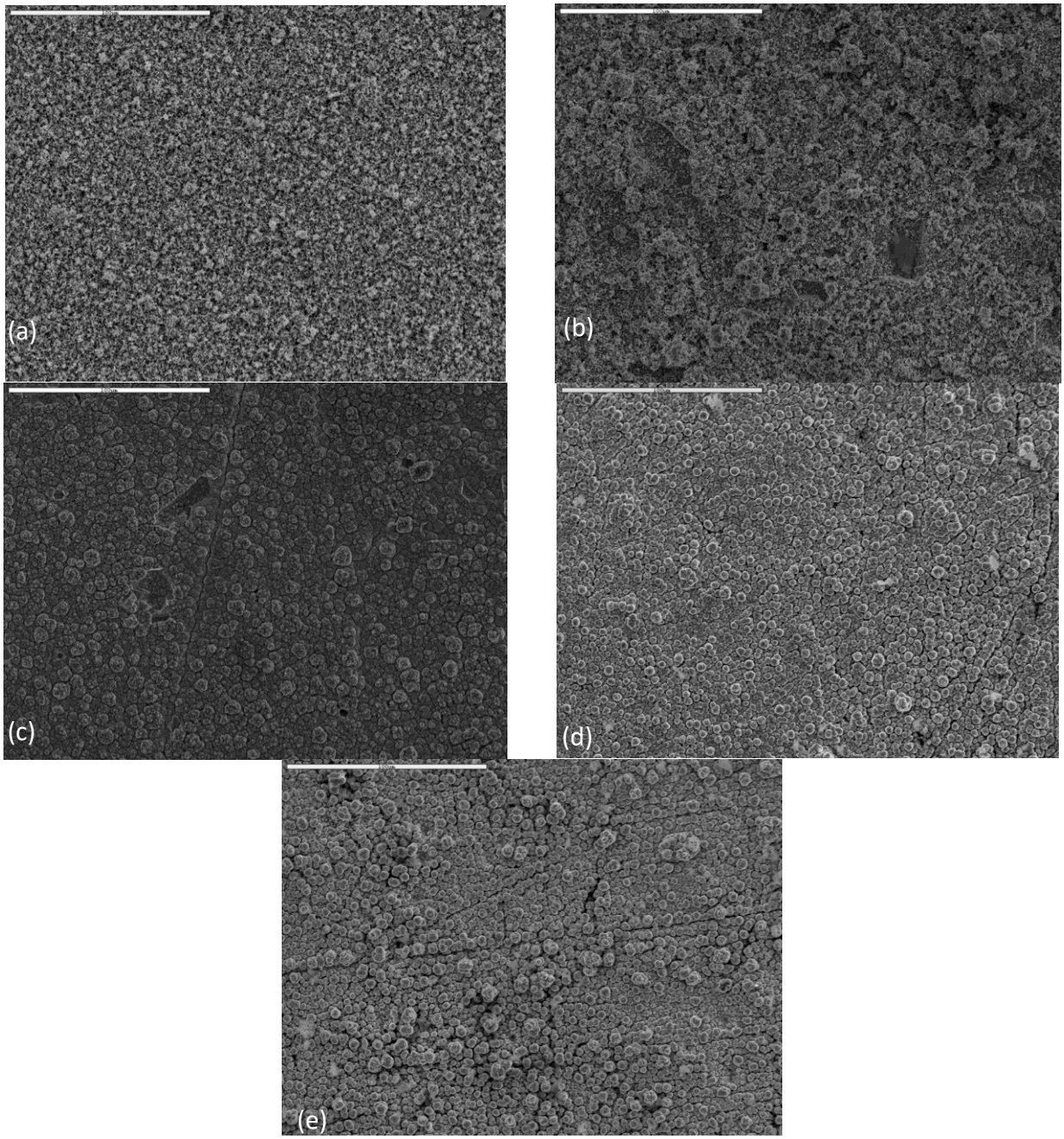

Figure 1. *Morphology of the Zn-Co-CeO_2 composite coatings deposited at: (a) 1, (b) 2, (c) 3, (d) 5 and (e) 8 A dm^{-2} from particles free plating solution ($CeCl_3$ as Ce source). Scale bars 100 µm*

The coatings produced through deposition using $CeCl_3$ as the source of cerium ions exhibit a significantly more compact structure. Microscopic imaging reveals that these coatings are more homogeneous at lower current densities of 1 and 2 A dm^{-2}. Even at elevated current densities, there is a lack of pronounced larger agglomerates, contrasting sharply with the coatings derived from biphasic plating solution, which display more pronounced agglomeration. Also, there is a lack of agglomerates on the surface of the composite coatings deposited from particles-free solution even

at 8 A dm^{-2}, which confirms the primary goal of this work. The reduction of the coating porosity is also more than evident when a particle-free plating bath is used ($CeCl_3$, Figure 1).

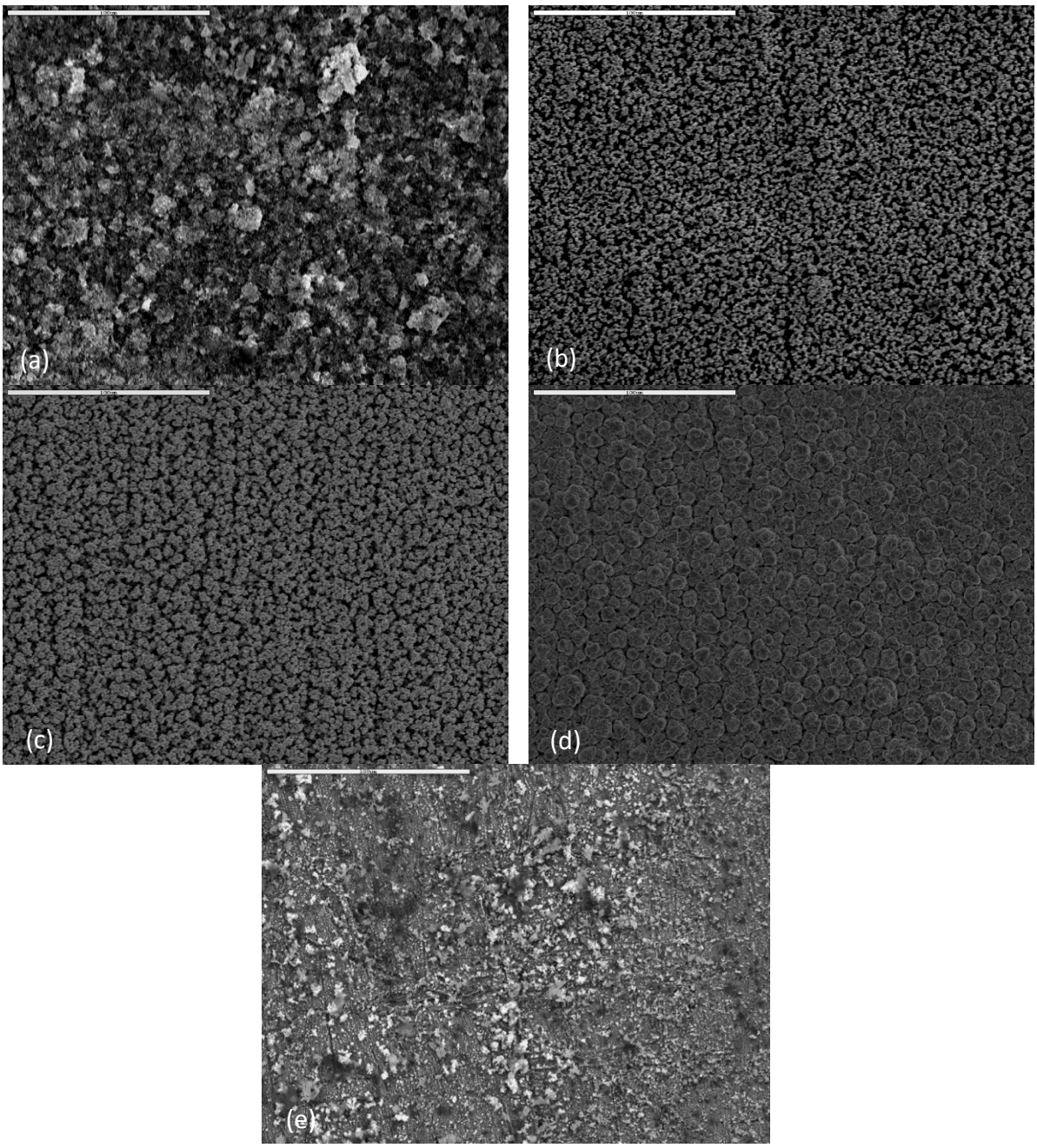

Figure 2. *Morphology of the Zn-Co-CeO_2 composite coatings deposited at: (a)1, (b) 2, (c) 3, (d) 5 and (e) 8 A dm^{-2} from plating solution with solid CeO_2 particles. Scale bars 100 µm*

This phenomenon arises from the distinct mechanisms of particle deposition. When using insoluble CeO_2 nanoparticles, agitation plays a crucial role in the codeposition process. The fluid flow predominantly transports the particles to the growing deposit layer, with electrophoresis contributing to a lesser extent. The nanoparticles are subsequently incorporated into the deposit primarily through entrapment within the growing layer. Conversely, when $CeCl_3$ is used, it dissolves in the plating solution. During the deposition process, specific local physico-chemical conditions at the zinc cobalt film interface promote the formation of a secondary phase consisting of cerium-based hydroxides. This occurs due to localized alkalinisation resulting from the reduction of dissolved oxygen and water, which can be described as a coprecipitation process [40]. The formed

cerium-hydroxide oxidizes to the CeO_2 [41,42]. As a result, the lack of microstress and internal straining within the coatings leads to a more homogeneous and compact structure.

The chemical composition of the composite coatings

The chemical content of composite coatings deposited from particle-free and biphasic plating solution as a function of the deposition current density is shown in Figure 3.

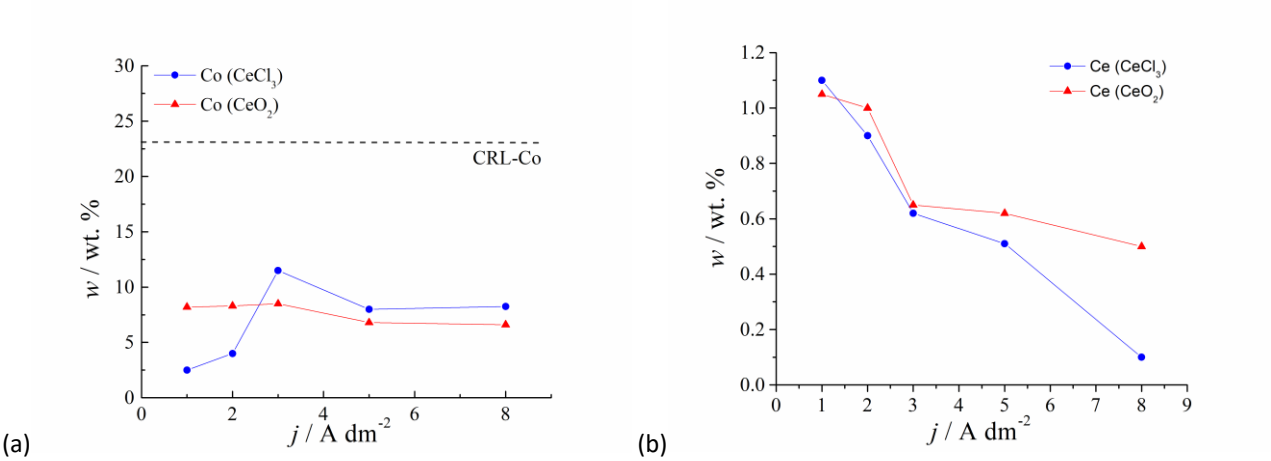

Figure 3. *Dependence of the (a) Co and (b) Ce contents in Zn-Co-CeO_2 coatings on the deposition current density for the coatings deposited from the particles free ($CeCl_3$ as a source of Ce) and biphasic plating solution (CeO_2 solid particles)*

From Figure 3(a), it can be noted that the cobalt content in the composite coatings increases with an increase in deposition current density when using $CeCl_3$ as Ce source, reaching a maximum of approximately 12 wt.% at j = 3 A dm^{-2}, after which it levels off. In contrast, the influence of current density on Co content in composites derived from biphasic plating solution (CeO_2 particles) is negligible. Brenner categorized the electrochemical deposition of Zn-Co alloys as anomalous, where zinc, being more electronegative, is preferentially deposited. The line labelled CRL-Co in Figure 3(a) serves as a control reference line, indicating the ratio of Co^{2+} ions to the total concentration of metal ions (Co^{2+} and Zn^{2+}) in the deposition solution. Since the Co content in the composite alloys deposited from both solutions is substantially below the CRL, we can infer that the deposition occurs via an anomalous mechanism and that the presence of the ceria in the solution does not affect the deposition process of the Zn-Co. The cerium (Ce) content in the coatings remains low (below 1.2 wt.%), which aligns with the low concentration of Ce in the deposition solution.

The use of a particles-free plating bath did not lead to an increase in cerium content in the composite coating, which is in agreement with existing literature [40]. Furthermore, higher cerium content does not necessarily correlate with improved properties, as morphology and compactness also play a significant role in determining coating performance. Scanning electron microscopy observations indicate that the use of a particle-free plating solution enhances the compactness and overall appearance of the coatings (Figure 1). Unlike Co, the Ce content decreases with increasing deposition current density in both solutions. During the initial stage of deposition, nucleation and growth of nuclei compete. At high current densities, the reaction rate is higher, leading to a nucleation rate surpassing the growth rate of the nuclei. Conversely, at low current densities, the growth rate of the nuclei predominates. Consequently, the enhanced deposition rate at higher current densities limits the ability of CeO_2 particles to be incorporated. The concentration of metal ions in the pre-electrode layer surpasses the particles, leading to a faster reduction of the metal ions.

Corrosion resistance of the composite coatings

The effects of using single versus biphasic plating solutions and variation of the deposition current densities on corrosion resistance and durability of the deposited composite coatings in a chloride-rich environment were evaluated by electrochemical impedance spectroscopy. The Nyquist diagrams, revealing the corrosion resistance of coatings produced at various current densities (1, 2, 3 and 5 A dm^{-2}) from biphasic plating solution in the presence of CeO_2, are illustrated in Figure 4(a), (c), (e) and (g). These diagrams exhibit two depressed semicircles, indicating two distinct time constants within the investigated frequency range. Notably, the diameter of the dominant semicircle, which represents the charge transfer process, increases upon exposure to NaCl solution. This impedance growth may be attributed to the formation of a pseudo-passive protective layer composed of corrosion products on the metal surface in contact with the corrosive medium, or it may reflect a self-healing effect of the substrate. Coatings deposited at a current density of 1 A dm^{-2} demonstrate significantly lower initial resistance compared to those obtained at 2 A dm^{-2}. Both samples exhibit an increase in resistance over the exposure to NaCl, with the coatings produced at 2 A dm^{-2} displaying superior corrosion stability. Coatings deposited at 3 A dm^{-2} exhibited lower impedance values compared to those obtained at 2 A dm^{-2}, although both showed an increase in impedance value over time. In contrast, the resistivity of coatings deposited at 5 A dm^{-2} consistently decreased over time, likely due to their inhomogeneous morphology, which includes porosity and defects. This structural irregularity may compromise the integrity of the protective layer, leading to reduced corrosion resistance.

Coatings produced with $CeCl_3$ as the source of cerium ions exhibited similar behaviour, as evidenced by the Nyquist diagrams in Figure 4(b), (d), (f), (h), although the resistivity of these samples was significantly higher compared to coatings produced from the biphasic plating solution. The durability of these coatings in aggressive corrosion media, like chloride-rich solution, was significantly increased. There could be several explanations for this phenomenon. The more homogenous morphology and increased compactness is surely one of the reasons, as a consequence of the utilization of the particle-free plating bath and suppressed incorporation of agglomerates inside the coating. In addition, since the deposition mechanism incorporating CeO_2 is changed in this case, a better distribution of the particles in the coatings is achieved. When homogeneously distributed cerium is throughout the coating, it could be accessible for the formation of CeO_2 through a pH-driven process [40], which, in turn, results in repairing the damage on the substrate surface after attack of the Cl^- anions and oxygen present in the corrosive media. Since ceria is known to have the self-healing effect [12,17,23,27,29], along with the passive layer formed on the coatings surfaces, it provided good corrosion protection during 2 weeks in NaCl solution for Zn-Co-CeO_2 coatings produced from particles free plating bath. The same coatings deposited from the biphasic plating solution were able to protect the steel only for up to 5 days in the same corrosive media.

For nearly all current densities tested, the impedance values for Zn-Co-CeO_2 coatings deposited from particle-free plating bath ($CeCl_3$) were higher than those for Zn-Co-CeO_2 coatings deposited from biphasic plating solution (CeO_2) (Figures 4 to 6). Notably, the coatings deposited at a current density of 3 A dm^{-2} showed the best performance, maintaining high resistance values throughout the 2-week testing period. The phase angle versus frequency diagrams clearly exhibit two time constants during the initial exposure to NaCl solution (Figures 5 and 6). The time constant observed at medium frequencies is associated with the resistance of solution penetration through the composite coating and the passive layer made of corrosion products formed on its surface [43].

The second time constant, occurring at lower frequencies, pertains to the electrochemical processes at the substrate/composite coating interface [44]. The Zn-Co-CeO_2 composite coatings result in only temporary corrosion protection of the underlying steel due to their porosity.

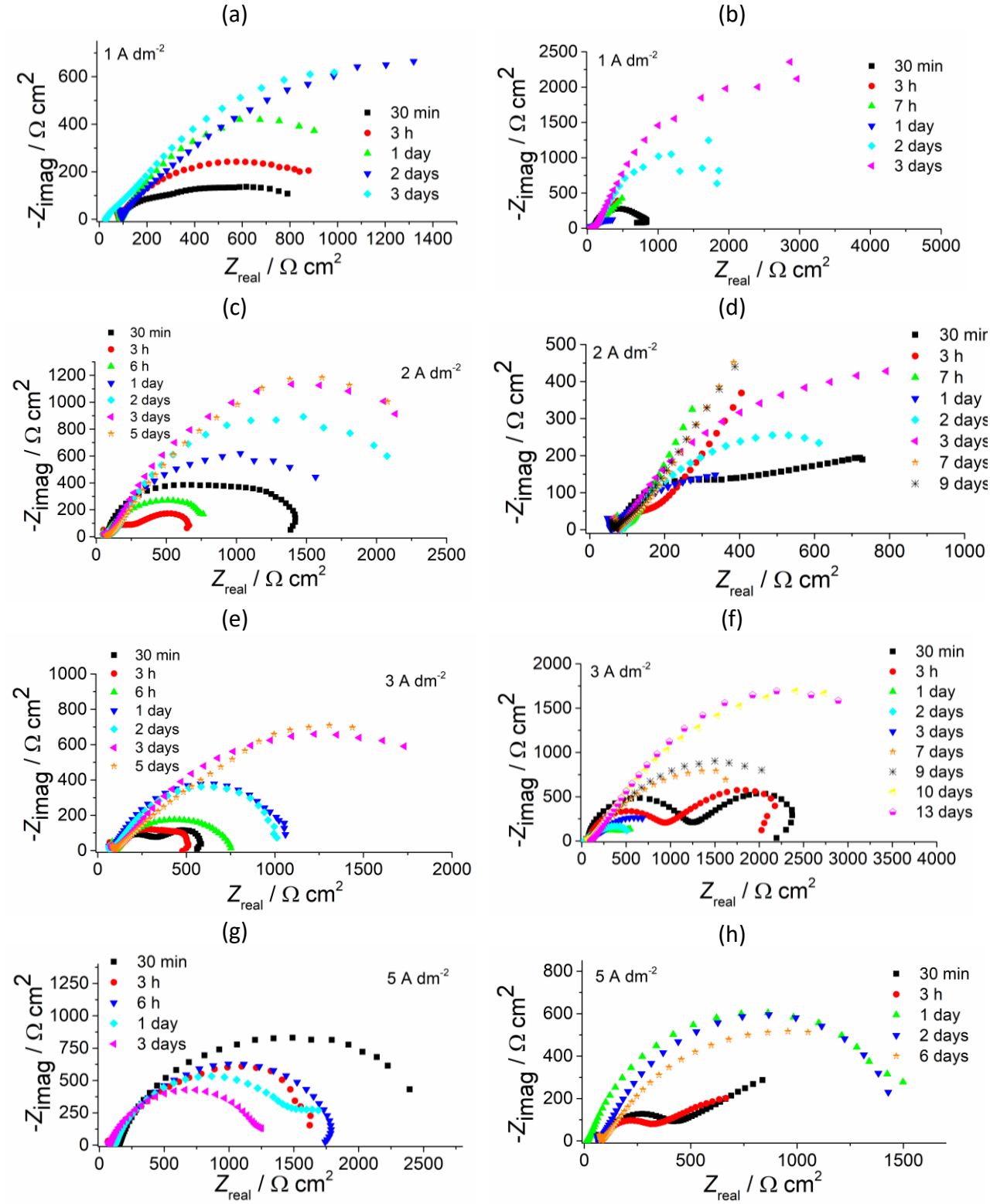

Figure 4. *Nyquist plots of composite coatings deposited at: 1 A dm^{-2} (a) from biphasic solution-CeO_2 particles, (b) particles free solution-$CeCl_3$; 2 A dm^{-2} (c) from biphasic solution, (d) particles free solution; 3 A dm^{-2} (e) from biphasic solution, (f) particles free solution; 5 A dm^{-2}, (g) from biphasic solution and (h) particles free solution*

The impedance values at low frequencies decreased in NaCl after some time (Figures 5 and 6), indicating electrolyte infiltration through the coating and subsequent corrosion progression.

(a)

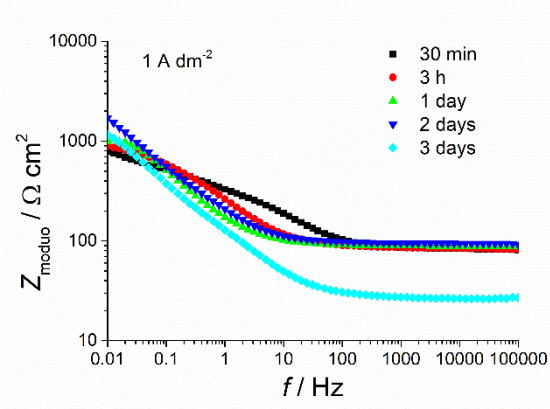
1 A dm-2
30 min
3 h
1 day
2 days
3 days
Zmoduo / Ω cm2
f / Hz

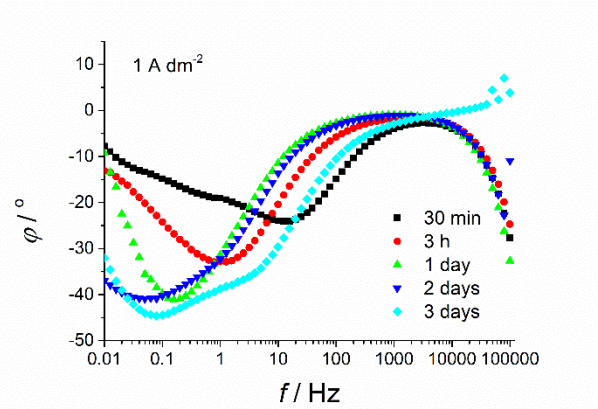
1 A dm-2
30 min
3 h
1 day
2 days
3 days
φ / °
f / Hz

(b)

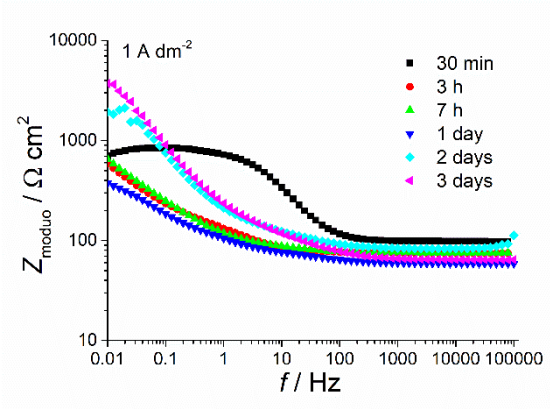
1 A dm-2
30 min
3 h
7 h
1 day
2 days
3 days
Zmoduo / Ω cm2
f / Hz

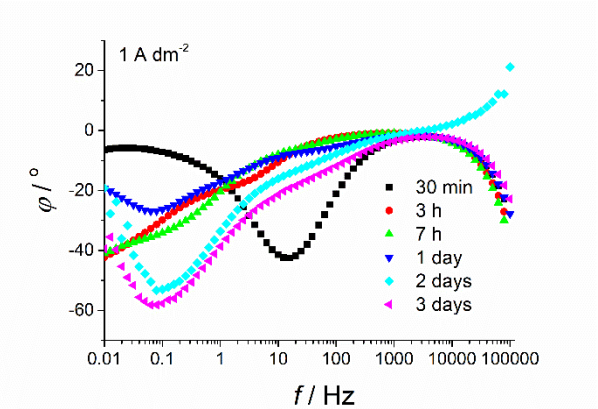
1 A dm-2
30 min
3 h
7 h
1 day
2 days
3 days
φ / °
f / Hz

(c)

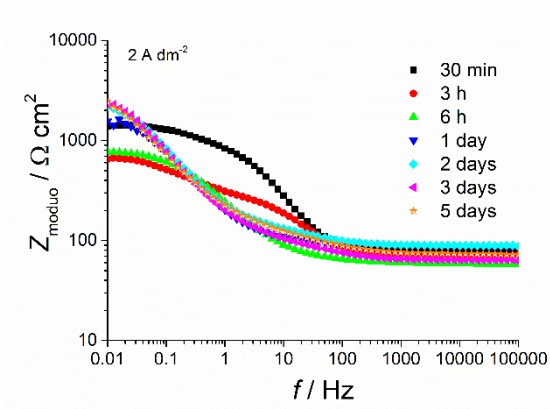
2 A dm-2
30 min
3 h
6 h
1 day
2 days
3 days
5 days
Zmoduo / Ω cm2
f / Hz

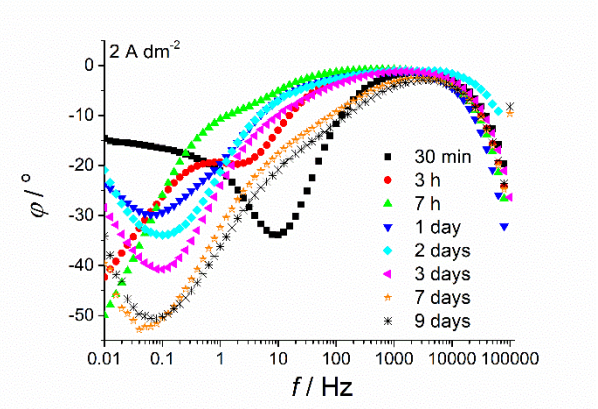
2 A dm-2
30 min
3 h
7 h
1 day
2 days
3 days
7 days
9 days
φ / °
f / Hz

(d)

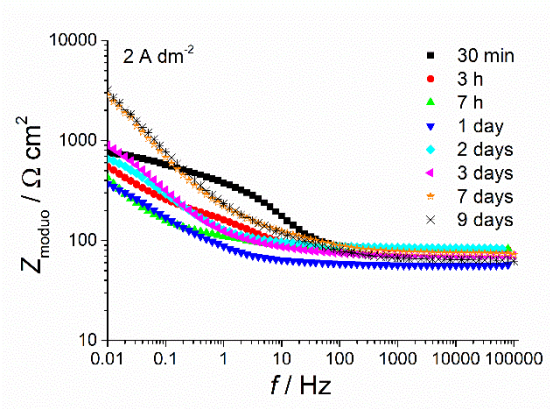
2 A dm-2
30 min
3 h
7 h
1 day
2 days
3 days
7 days
9 days
Zmoduo / Ω cm2
f / Hz

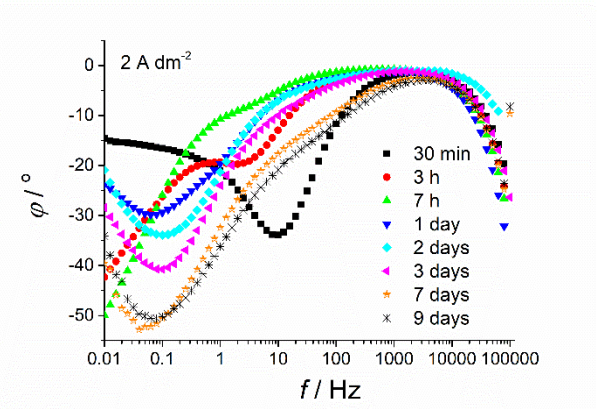
2 A dm-2
30 min
3 h
7 h
1 day
2 days
3 days
7 days
9 days
φ / °
f / Hz

Figure 5. *Bode plots of composite coatings deposited at 1 A dm^{-2} (a) from biphasic plating solution-CeO_2 particles, (b) particles free solution -$CeCl_3$; 2 A dm^{-2} (c) from biphasic plating solution, (d) particles free solution; 3 A dm^{-2}*

(a)

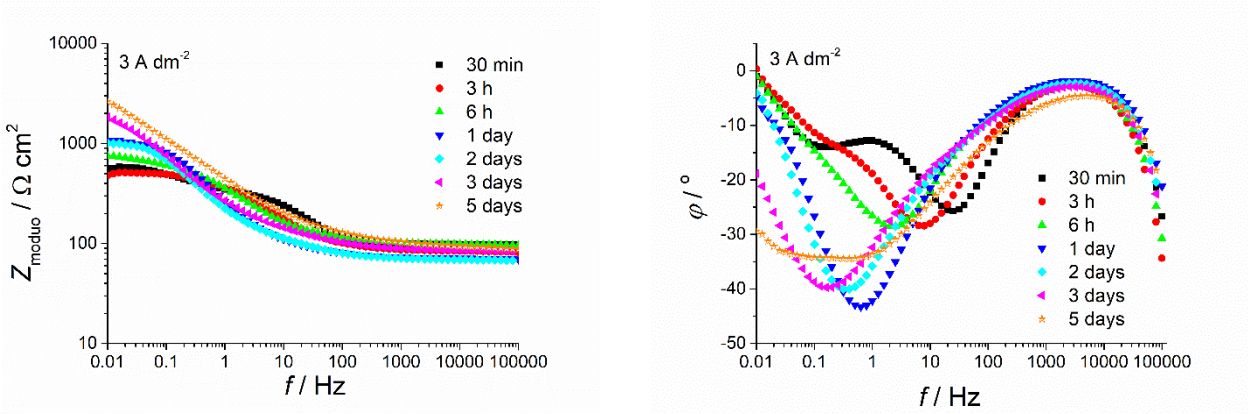

(b)

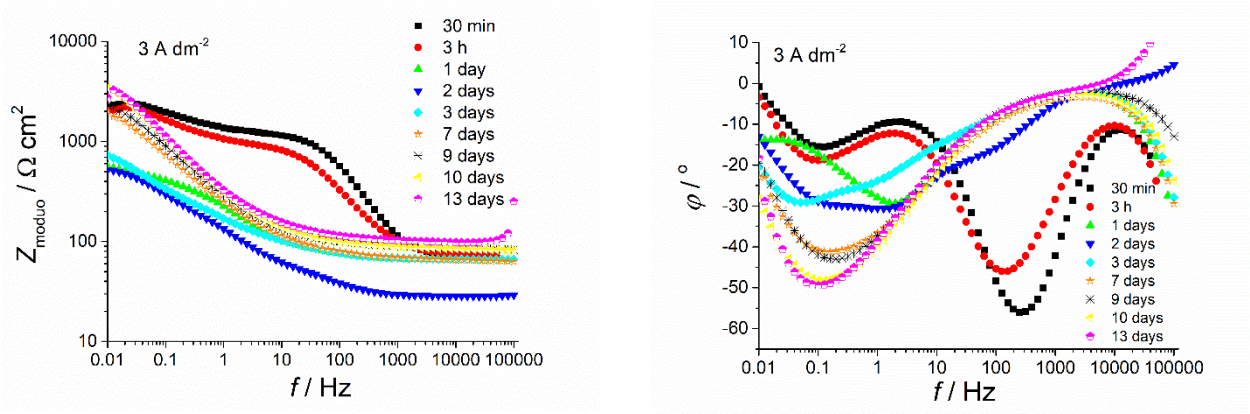

(c)

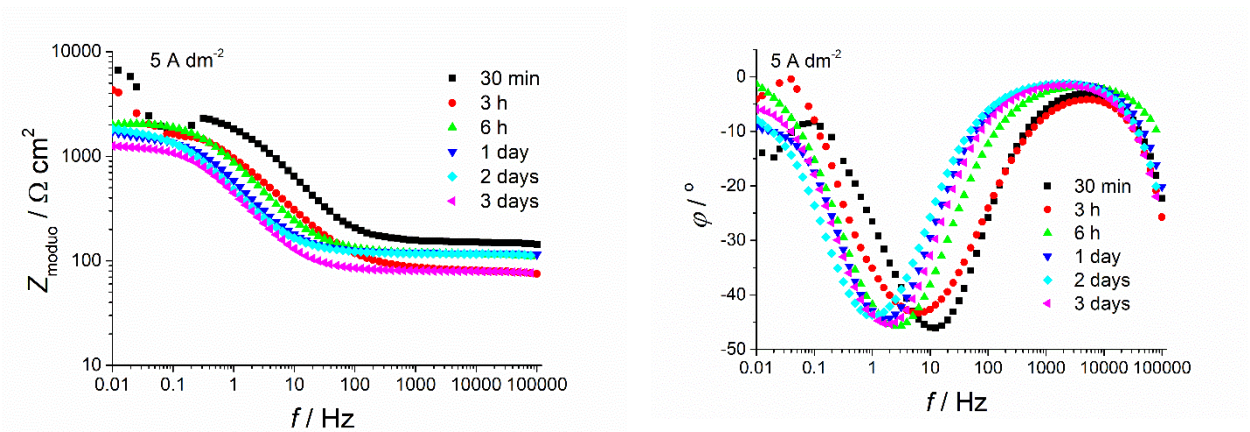

(d)

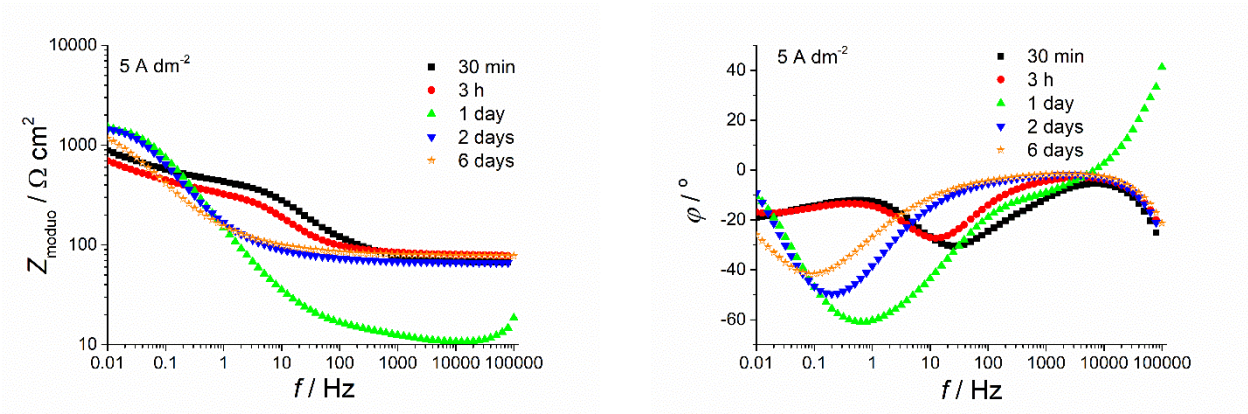

Figure 6. *Bode plots of composite coatings deposited at: 1 A dm^{-2} (a) from biphasic plating solution, (b) particles free solution; 5 A dm^{-2} (c) from biphasic plating solution, (d) particles free solution*

However, over a longer time in the NaCl environment, the impedance values at low frequencies increase again, and only the second time constant remains visible. Eventually, the phase angle exhibits a single maximum position between the original two. This behaviour is often characteristic of coatings that facilitate a self-healing effect. As the electrolyte continued to penetrate, CeO_2 particles diffused through the coating and accumulated at the active sites on the steel substrate. Given that CeO_2 has a low solubility [44], the observed high impedance values at low frequencies are to be expected. This behaviour suggests that the presence of CeO_2 particles contributes to the formation of a protective layer that enhances the corrosion resistance of the substrate. By fitting the obtained EIS results using the equivalent electrical circuits shown in Figure 7, where R_Ω denotes the solution resistance, R_p is the resistance of the coating, C_c capacitance of the coating, CPE denotes the constant phase element corresponding to the double layer capacitance in parallel with the charge transfer resistance (R_{ct}), it is possible to determine the charge transfer resistance values.

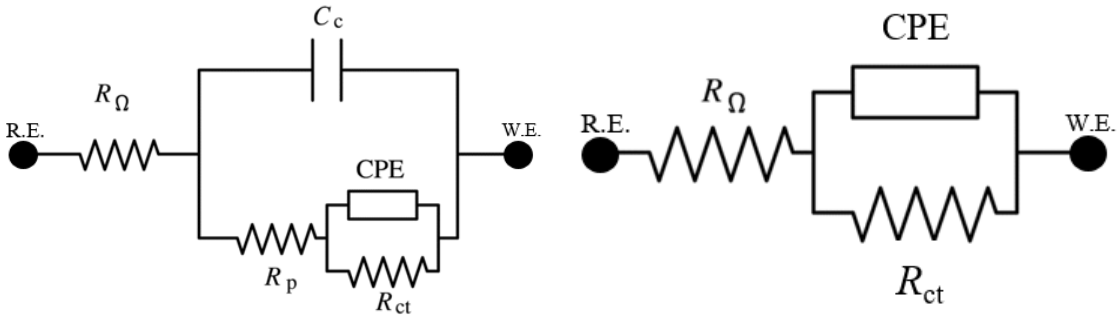

Figure 7. *Equivalent electric circuits used for fitting the electrochemical impedance data; R.E. reference electrode, W.E. working electrode*

Figure 8 illustrates the dependence of R_{ct} values on the exposure time of the coatings deposited at various current densities (1, 2, 3, and 5 A dm^{-2}) and from different plating solutions (containing CeO_2 or $CeCl_3$) to the NaCl solution. Initially, all tested coatings at all current densities exhibit a decrease in R_{ct} values, which can be attributed to the contact of the metal surface with the electrolyte. After a certain exposure time, the R_{ct} values of the composite coatings begin to increase and then stabilize, reaching a plateau of nearly constant values. This behaviour suggests a gradual development of a protective layer, enhancing the corrosion resistance of the coatings over time. The plateau in R_{ct} values corresponds to the formation of a passive layer of corrosion products on the metal surface, effectively hindering further substrate activity.

Notably, significantly higher R_{ct} values were observed for the Zn-Co-CeO_2 composite coating produced from particle-free plating solution compared to the Zn-Co-CeO_2 coating from the biphasic solution, confirming the superior corrosion stability of the coatings derived from $CeCl_3$ containing bath. The persistence of this phenomenon over extended exposure to NaCl suggests the presence of a layer with a low solubility product from the CeO_2 layer, indicative of a self-healing effect of the substrate. Based on the EIS results, it can be concluded that composite coatings based on Zn-Co alloy and cerium obtained from $CeCl_3$ exhibit better corrosion stability than those deposited from CeO_2 based bath. When CeO_2 particles are utilized for composite alloy formation, they tend to precipitate at the site of damage, where corrosion processes have initiated, likely forming a physisorbed layer of CeO_2. In contrast, the cerium-based layer produced via a pH-driven process in coatings produced from solution with $CeCl_3$ appears to provide enhanced protection. Cerium can undergo oxidation-reduction cycles between Ce(III) and Ce(IV) due to the presence of oxygen vacancies and the small energy difference between its 4f inner and outer valence electrons [45]. The Ce(IV) hydroxides begin to precipitate around pH 4 [46], while Ce(III) hydroxides start to form at around pH 8 [46]. These hydroxides serve as reaction intermediates for the formation of CeO_2. In CeO_2, cerium atoms predominantly exist in the +4 oxidation state. However, the presence of missing lattice oxygen atoms in this highly reducible oxide indicates that two Ce(III) ions are situated near each oxygen vacancy [45]. Thus, the formed protection layer always consists of a mixture of Ce(III) and Ce(IV) species, along with Zn and Co oxides/hydroxides. A key factor in the superior performance of the CeO_2 layer is its adhesion to the metal substrate, which is likely stronger when formed in situ from Ce(III) through a pH-driven process. In contrast, CeO_2 particles precipitated from the alloy during corrosion may not bond as effectively with the substrate.

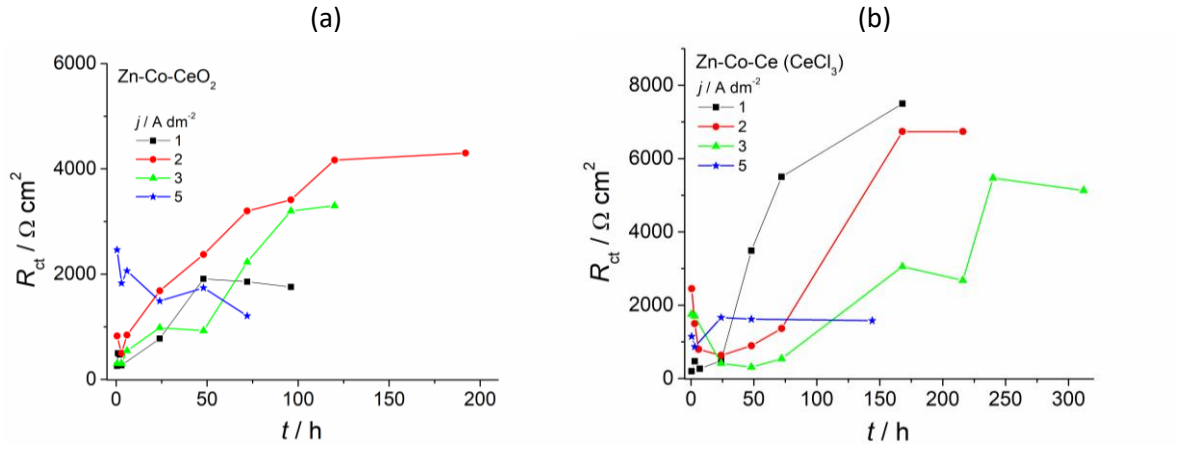

Figure 8. *Charge transfer resistance values (R_{ct}) of composite coatings deposited from (a) biphasic plating solution - CeO_2 particles and (b) single plating solution - $CeCl_3$ as Ce source*

Conclusions

The results shown indicate that deposition current density significantly influences the morphology, chemical composition, and corrosion resistance of composite coatings, irrespective of the particle source. Specifically, lower current densities yield finer-grained coatings with strong adhesion to the substrate and enhanced compactness. In contrast, higher current densities produce uneven coatings that exhibit reduced compactness and visible surface porosity as a consequence of uneven current distribution. Additionally, increased current density correlates with lower incorporation of CeO_2 particles within the coating. Given that cobalt concentrations were significantly below the critical reduction limit, the presence of particles in the plating solution did

not alter the deposition mechanism of the Zn-Co alloy, which remained anomalous regardless of the ceria source. Utilizing a single plating solution effectively suppressed particle agglomeration, resulting in coatings that were more homogeneous, denser, and demonstrated improved corrosion resistance and durability due to their self-healing ability in chloride-rich environments.

Acknowledgements: The Ministry of Scientific and Technological Development and Higher Education of the Republic of Srpska (Grant No. 19.032/431-1-34/23) and the Ministry of Science, Technological Development and Innovation of the Republic of Serbia (Contract No. 451-03-65/2024-03/200135) are gratefully acknowledged for funding this research.

References

[1] A. Vlasa, S. Varvara, A. Pop, C. Bulea, L. M. Muresan, Electrodeposited Zn–TiO_2 nanocomposite coatings and their corrosion behavior, *Journal of Applied Electrochemistry* **40** (2010) 1519-1527. https://doi.org/10.1007/s10800-010-0130-x

[2] K. Vathsala, T. V. Venkatesha, Zn–ZrO_2 nanocomposite coatings: Elecrodeposition and evaluation of corrosion resistance, *Applied Surface Science* **257(21)** (2011) 8929-8936. https://doi.org/10.1016/j.apsusc.2011.05.0

[3] M. Sajjadnejad, S. Karkon, S. M. S. Haghshenas, Corrosion characteristics of Zn-TiO_2 nanocomposite coatings fabricated by electro-codeposition process, *Advanced Journal of Chemistry A* **7(2)** (2024) 209-226. https://doi.org/10.48309/ajca.2024.418391.1425

[4] K. K. Maniam, S. Paul, Corrosion performance of electrodeposited zinc and zinc-alloy coatings in marine environment, *Corrosion and Materials Degradation* **2(2)** (2021) 163-189. https://doi.org/10.3390/cmd2020010

[5] C. M. P. Kumar, A. Lakshmikanthan, M. P. G. Chandrashekarappa, D. Y. Pimenov, K. Giasin, Electrodeposition based preparation of Zn–Ni alloy and Zn–Ni–WC nanocomposite coatings for corrosion-resistant applications, *Coatings* **11(6)** (2021) 712. https://doi.org/10.3390/coatings11060712

[6] M. Klekotka, K. Zielińska, A. Stankiewicz, M. Kuciej, Tribological and anticorrosion performance of electroplated zinc based nanocomposite coatings, *Coatings* **10)6)** (2020) 594. https://doi.org/10.3390/coatings10060594

[7] M. Egbuhuzor, C. Akalezi, S. Ulaeto, D. Njoku, B. Onyeachu, E. Oguzie, Electro-deposited nanocomposite coatings and their behaviours against aqueous and high-temperature corrosion: A review, *Hybrid Advances* **5** (2024) 100180. https://doi.org/10.1016/j.hybadv.2024.100180

[8] A. Cabral, A. O. Junior, G. Koga, I. Rigoli, C. Rocha, C. Souza, Electrodeposited Zinc Cellulose Nanocrystals Composite Coatings: Morphology, Structure, Corrosion Resistance and Electrodeposition Process, *Journal of Materials Research and Technology* **33** (2024) 1569-1580 https://doi.org/10.1016/j.jmrt.2024.09.153

[9] M. M. K. Azar, H. S. Gugtapeh, M. Rezaei, Evaluation of corrosion protection performance of electroplated zinc and zinc-graphene oxide nanocomposite coatings in air saturated 3.5 wt.% NaCl solution, *Colloids and Surfaces A: Physicochemical and Engineering Aspects* **601** (2020) 125051. https://doi.org/10.1016/j.colsurfa.2020.125051

[10] S. Anwar, F. Khan, Y. Zhang, Corrosion behaviour of Zn-Ni alloy and Zn-Ni-nano-TiO_2 composite coatings electrodeposited from ammonium citrate baths, *Process Safety and Environmental Protection* **141** (2020) 366-379. https://doi.org/10.1016/j.psep.2020.05.048

[11] H. Srivastav, A. Z. Weber, C. J. Radke, Colloidal Stability of PFSA-Ionomer Dispersions. Part I. Single-Ion Electrostatic Interaction Potential Energies, *Langmuir* **40(13)** (2024) 6654-6665. https://pubs.acs.org/doi/abs/10.1021/acs.langmuir.3c03903

[12] M. Riđošić, M. Bučko, A. Salicio-Paz, E. García-Lecina, L. S. Živković, J. B. Bajat, Ceria particles as efficient dopant in the electrodeposition of Zn-Co-CeO_2 composite coatings with

enhanced corrosion resistance: The effect of current density and particle concentration, *Molecules* **26(15)** (2021) 4578. https://doi.org/10.3390/molecules26154578

[13] R. Daneshfar, B. S. Soulgani, S. Ashoori, Identifying the mechanisms behind the stability of silica nano-and micro-particles: effects of particle size, electrolyte concentration and type of ionic species, *Journal of Molecular Liquids* **397** (2024) 124059. https://doi.org/10.1016/j.molliq.2024.124059

[14] X. Wang, T. Sun, H. Zhu, T. Han, J. Wang, H. Dai, Roles of pH, cation valence, and ionic strength in the stability and aggregation behavior of zinc oxide nanoparticles, *Journal of Environmental Management* **267** (2020) 110656. https://doi.org/10.1016/j.jenvman.2020.110656

[15] M. Riđošić, A. Salicio-Paz, E. Garcia-Lecina, P. Zabinski, L. S. Živković, J. B. Bajat, The effect of the ultrasound agitation and source of ceria particles on the morphology and structure of the Zn–Co–CeO_2 composite coatings, *Journal of Materials Research and Technology* **13** (2021) 1336-1349. https://doi.org/10.1016/j.jmrt.2021.05.064

[16] M. Bucko, M. Riđošić, J. Kovačina, M. Tomić, J. Bajat, Hardness and corrosion resistance of Zn− Mn/Al_2O_3 composite coatings produced by electrochemical deposition, *Indian Journal of Engineering and Materials Sciences* **29(4)** (2022) 540-549. http://op.niscpr.res.in/index.php/IJEMS/article/view/47785/0

[17] M. Riđošić, N. D. Nikolić, A. Salicio-Paz, E. García-Lecina, L. S. Živković, J. B. Bajat, Zn-Co-CeO_2 vs. Zn-Co Coatings: Effect of CeO_2 Sol in the Enhancement of the Corrosion Performance of Electrodeposited Composite Coatings, *Metals* **11(5)** (2021) 704. https://doi.org/10.3390/met11050704

[18] J. M. Costa, A. F. de Almeida Neto, Ultrasound-assisted electrodeposition and synthesis of alloys and composite materials: A review, *Ultrasonics Sonochemistry* **68** (2020) 105193. https://doi.org/10.1016/j.ultsonch.2020.105193

[19] M. Akbarpour, F. G. Asl, Fabrication of high-performance graphene/nickel-cobalt composite coatings using ultrasonic-assisted pulse electrodeposition, *Ceramics International* **49(9)** (2023) 13829-13835. https://doi.org/10.1016/j.ceramint.2022.12.262

[20] C. Liu, X. Huang, R. Xu, Y. Mai, L. Zhang, X. Jie, Microstructure and properties of nanocrystalline Ni-Mo coatings prepared by ultrasound-assisted pulse electrodeposition, *Journal of Materials Engineering and Performance* **30** (2021) 2514-2525. https://doi.org/10.1007/s11665-021-05570-1

[21] H. Zhang, J. Wang, S. Chen, H. Wang, Y. He, C. Ma, Ni–SiC composite coatings with improved wear and corrosion resistance synthesized via ultrasonic electrodeposition, *Ceramics International* **47(7)** (2021) 9437-9446. https://doi.org/10.1016/j.ceramint.2020.12.076

[22] C. Ma, D. Zhao, F. Xia, H. Xia, T. Williams, H. Xing, Ultrasonic-assisted electrodeposition of Ni-Al_2O_3 nanocomposites at various ultrasonic powers, *Ceramics International* **46(5)** (2020) 6115-6123. https://doi.org/10.1016/j.ceramint.2019.11.075

[23] X. Gong, M. Luo, M. Wang, W. Niu, Y. Wang, B. Lei, Injectable self-healing ceria-based nanocomposite hydrogel with ROS-scavenging activity for skin wound repair, *Regenerative Biomaterials* **9** (2022) rbab074. https://doi.org/10.1093/rb/rbab074

[24] S. V. Harb, A. Trentin, T. A. C. de Souza, M. Magnani, S. H. Pulcinelli, C. V. Santilli, P. Hammer, Effective corrosion protection by eco-friendly self-healing PMMA-cerium oxide coatings, *Chemical Engineering Journal* **383** (2020) 123219. https://doi.org/10.1016/j.cej.2019.123219

[25] V. Hernández-Montes, R. Buitrago-Sierra, M. Echeverry-Rendón, J. Santa-Marín, Ceria-based coatings on magnesium alloys for biomedical applications: a literature review, *RSC Advances* **13(2)** (2023) 1422-1433. https://doi.org/10.1039/D2RA06312C

[26] B. Fotovvat, M. Behzadnasab, S. Mirabedini, H. E. Mohammadloo, Anti-corrosion performance and mechanical properties of epoxy coatings containing microcapsules filled

with linseed oil and modified ceria nanoparticles, *Colloids and Surfaces A: Physicochemical and Engineering Aspects* **648** (2022) 129157. https://doi.org/10.1016/j.colsurfa.2022.129157
[27] S. Habib, E. Fayyad, M. Nawaz, A. Khan, R. A. Shakoor, R. Kahraman, A. Abdullah, Cerium dioxide nanoparticles as smart carriers for self-healing coatings, *Nanomaterials* **10(4)** (2020) 791. https://doi.org/10.3390/nano10040791
[28] H. Zhang, H. Bian, X. Zhang, L. Zhang, Y. Chen, Y. Yang, Z. Zhang, Preparation and characterization of hollow ceria based smart anti-corrosive coatings on copper, *Surfaces and Interfaces* **45** (2024) 103930. https://doi.org/10.1016/j.surfin.2024.103930
[29] A. Kirdeikiene, O. Girčiene, L. Gudavičiūte, V. Jasulaitiene, A. Selskis, S. Tutliene, M. Skruodiene, J. Pilipavičius, J. Juodkazyte, R. Ramanauskas, Self-healing properties of cerium-modified molybdate conversion coating on steel, *Coatings* **11(2)** (2021) 194. https://doi.org/10.3390/coatings11020194
[30] S. V. Kozhukharov, C. Girginov, N. Boshkova, A. Tzanev, Impact of the final thermal sealing of combined zinc/cerium oxide protective coating primers formed on low carbon steel. *Journal of Electrochemical Science and Engineering* **12(4)** (2022) 685-701. http://dx.doi.org/10.5599/jese.1297
[31] J. Gulicovski, J. Bajat, V. Mišković-Stanković, B. Jokić, V. Panić, S. Milonjić, Cerium oxide as conversion coating for the corrosion protection of aluminum, *Journal of Electrochemical Science and Engineering* **3(4)** (2013) 151-156. https://doi.org/10.5599/jese.2013.0037
[32] L. Exbrayat, C. Rébéré, R. Milet, E. Calvié, P. Steyer, J. Creus, Corrosion Behavior in Saline Solution of Electrodeposited Nanocomposite Zn-CeO_2 Coatings Deposited onto Low Alloyed Steel, *Coatings* **13(10)** (2023) 1688. https://doi.org/10.3390/coatings13101688
[33] P. I. Nemes, M. Lekka, L. Fedrizzi, L. M. Muresan, Influence of the electrodeposition current regime on the corrosion resistance of Zn-CeO_2 nanocomposite coatings, *Surface and Coatings Technology* **252** (2014) 102-107. https://doi.org/10.1016/j.surfcoat.2014.04.051
[34] S. Ranganatha, T. Venkatesha, K. Vathsala, Electrochemical studies on Zn/nano-CeO_2 electrodeposited composite coatings, *Surface and Coatings Technology* **208** (2012) 64-72. https://doi.org/10.1016/j.surfcoat.2012.08.004
[35] S. Lajevardi, T. Shahrabi, Effects of pulse electrodeposition parameters on the properties of Ni–TiO_2 nanocomposite coatings, *Applied Surface Science* **256(22)** (2010) 6775-6781. https://doi.org/10.1016/j.apsusc.2010.04.088
[36] E. Beltowska-Lehman, P. Indyka, A. Bigos, M. J. Szczerba, J. Guspiel, H. Koscielny, M. Kot, Effect of current density on properties of Ni–W nanocomposite coatings reinforced with zirconia particles, *Materials Chemistry and Physics* **173** (2016) 524-533. https://doi.org/10.1016/j.matchemphys.2016.02.050
[37] Z. Zhang, B. Li, S. Chen, Z. Yuan, C. Xu, W. Zhang, Influences of Al particles and current density on structural, mechanical and anti-corrosion properties of electrodeposited Ni–Co/Al composite coatings, *Ceramics International* **50(7)** (2024) 11804-11816. https://doi.org/10.1016/j.ceramint.2024.01.085
[38] F. Walsh, C. Ponce de Leon, A review of the electrodeposition of metal matrix composite coatings by inclusion of particles in a metal layer: an established and diversifying technology, *Transactions of the IMF* **92(5)** (2014) 83-98. https://doi.org/10.1179/0020296713Z.000000000161
[39] T. J. Tuaweri, G. D. Wilcox, Influence of SiO_2 particles on zinc–nickel electrodeposition, *Transactions of the IMF* **85(5)** (2007) 245-253. https://doi.org/10.1179/174591907X229608
[40] L. Exbrayat, J. Creus, Synthesis of Zn-Ceria Nanocomposite Coatings from Particle-Free Aqueous Bath in a one Electrodeposition Step Process, *Colloid and Interface Science Communications* **25** (2018) 31-35. https://doi.org/https://doi.org/10.1016/j.colcom.2018.06.004

[41] Y. Hamlaoui, F. Pedraza, C. Remazeilles, S. Cohendoz, C. Rébéré, L. Tifouti, J. Creus, Cathodic electrodeposition of cerium-based oxides on carbon steel from concentrated cerium nitrate solutions: Part I. Electrochemical and analytical characterisation, *Materials Chemistry and Physics* **113(2)** (2009) 650-657. https://doi.org/https://doi.org/10.1016/j.matchemphys.2008.08.027

[42] L. Martínez, E. Román, J. L. de Segovia, S. Poupard, J. Creus, F. Pedraza, Surface study of cerium oxide based coatings obtained by cathodic electrodeposition on zinc, *Applied Surface Science* **257(14)** (2011) 6202-6207. https://doi.org/https://doi.org/10.1016/j.apsusc.2011.02.033

[43] A. M. Simões, J. Torres, R. Picciochi, J. C. S. Fernandes, Corrosion inhibition at galvanized steel cut edges by phosphate pigments, *Electrochimica Acta* **54(15)** (2009) 3857-3865. https://doi.org/10.1016/j.electacta.2009.01.065

[44] T. V. Plakhova, A. Y. Romanchuk, S. N. Yakunin, T. Dumas, S. Demir, S. Wang, S. G. Minasian, D. K. Shuh, T. Tyliszczak, A. A. Shiryaev, A. V. Egorov, V. K. Ivanov, S. N. Kalmykov, Solubility of Nanocrystalline Cerium Dioxide: Experimental Data and Thermodynamic Modeling, *The Journal of Physical Chemistry C* **120(39)** (2016) 22615-22626. https://doi.org/10.1021/acs.jpcc.6b05650

[45] C. E. Castano, M. J. O'Keefe, W. G. Fahrenholtz, Cerium-based oxide coatings, *Current Opinion in Solid State and Materials Science* **19(2)** (2015) 69-76. https://doi.org/10.1016/j.cossms.2014.11.005

[46] B. Bouchaud, J. Balmain, G. Bonnet, F. Pedraza, pH-distribution of cerium species in aqueous systems, *Journal of Rare Earths* **30(6)** (2012) 559-562. https://doi.org/10.1016/S1002-0721(12)60091-X

[47] S. A. Hayes, P. Yu, T. J. O'Keefe, M. J. O'Keefe, J. O. Stoffer, The Phase Stability of Cerium Species in Aqueous Systems : I. E-pH Diagram for the System Ce-$HClO_4$-H_2O system, *Journal of The Electrochemical Society* **149(12)** (2002) C623-C630. https://doi.org/10.1149/1.1516775